Monte Carlo simulation and molecular theory of tethered polyelectrolytes

Owen J. Hehmeyer, Gaurav Arya, and Athanassios Z. Panagiotopoulos
Department of Chemical Engineering, Princeton University, Princeton, New Jersey 08544

Igal Szleifer
Department of Chemistry, Purdue University, West Lafayette, Indiana 47907

(Received 26 March 2007; accepted 15 May 2007; published online 28 June 2007)

We investigate the structure of end-tethered polyelectrolytes using Monte Carlo simulations and molecular theory. In the Monte Carlo calculations we explicitly take into account counterions and polymer configurations and calculate electrostatic interaction using Ewald summation. Rosenbluth biasing, distance biasing, and the use of a lattice are all used to speed up Monte Carlo calculation, enabling the efficient simulation of the polyelectrolyte layer. The molecular theory explicitly incorporates the chain conformations and the possibility of counterion condensation. Using both Monte Carlo simulation and theory, we examine the effect of grafting density, surface charge density, charge strength, and polymer chain length on the distribution of the polyelectrolyte monomers and counterions. For all grafting densities examined, a sharp decrease in brush height is observed in the strongly charged regime using both Monte Carlo simulation and theory. The decrease in layer thickness is due to counterion condensation within the layer. The height of the polymer layer increases slightly upon charging the grafting surface. The molecular theory describes the structure of the polyelectrolyte layer well in all the different regimes that we have studied. © *2007 American Institute of Physics*. [DOI: 10.1063/1.2747600]

I. INTRODUCTION

Grafted polyelectrolyte systems are widespread in nature. Within the human body, polyelectrolytes are found lubricating the joints and attached to the surface of cells. Inspired by biological systems, scientists are trying to reduce mechanical wear using lubrication by polyelectrolytes.[1] Thermally[2] and electrically responsive[3] polyelectrolyte brushes have also been created and may be useful in sensor applications. Recent reviews[4–6] summarize much of the progress on grafted and ungrafted polyelectrolytes.

For neutral polymers in good solvents, entropic forces due to volume exclusion determine the structure, and the configurations are self-avoiding random walks.[7] The behavior of neutral, grafted polymers on a single wall are determined by the interplay between the elastic entropy of the chains and the intermolecular excluded volume. The structural and thermodynamic properties of these systems have been explained in previous work utilizing scaling,[8,9] analytical self-consistent field theory, numerical self-consistent field, and molecular theories,[10–13] as well as molecular dynamics and Monte Carlo simulations[12–15] (for reviews see Refs. 10, 16, and 17). Polyelectrolytes present the additional complexity of electrostatic forces. The structure of a polyelectrolyte brush is determined by a competition between Coulomb repulsion among the chains that tends to straighten them and a moderation of this effect by counterions that screen the charged monomer interactions. Excluded volume effects become important at high grafting densities. The competition between excluded volume and electrostatic interactions is rather complex, and a complete understanding of the structural features of end-grafted polyelectrolytes has not yet been attained. However, there have been some insightful studies that have provided the basic understanding of these systems. These approaches include scaling theories,[4,18,19] and numerical self-consistent field approaches. Israëls *et al.*[20] used a lattice self-consistent field theory to examine the effect of salt on weakly charged unquenched polyelectrolytes on uncharged walls. Von Goeler and Muthukumar[21] developed a self-consistent field theory and studied the role of salt concentration and short range repulsive interactions on the density profiles of the brushes. Borisov *et al.*[22] have examined weakly charged quenched polyelectrolytes attached to a solid charged surface. For a review see Refs. 4 and 5.

The purpose of this work is to study the structure of end-grafted short polyelectrolytes using accurate Monte Carlo simulations and a molecular theory. The specific systems of interest are unsalted tethered layers composed of short chains. Most of the work on polyelectrolyte brushes concentrates on the long chain limit. However, there is a large range of experimental systems in which the understanding of the properties of relatively short chains is important. Short chain systems include self-assembled monolayers[3] and brushes composed of DNA used for sensing and detection.[23] In the limit of short chains the molecular details become important, and thus analytical approaches based on infinitely long chains have to be considered with care. The Monte Carlo technique provides nearly exact properties of the model system, and a comparison with the molecular theory provides the means to determine the quality of the approximations used in its derivation. The comparison of these approaches with analytical predictions provides the complete spectrum of the ranges, where each theoretical approach can be applied.

 © 2007 American Institute of Physics

Downloaded 28 Jun 2007 to 128.220.135.141. Redistribution subject to AIP license or copyright, see http://jcp.aip.org/jcp/copyright.jsp

An end-tethered polymer layer with a fixed monomer charge, independent of the *p*H of the solution, is called a quenched brush. All of the systems examined in this work are quenched brushes with no added salt. According to the scaling theory,[24] unsalted quenched brushes may exist in the quasineutral, osmotic, or Pincus regimes, and also perhaps in a collapsed regime. If excluded volume effects dominate over electrostatic effects, as occurs at very high grafting densities, the brush height scales as it does for neutral brushes, and this regime is called the "quasineutral" regime. For neutral brushes, the height of the brush goes as $h \propto N\sigma_g^{1/3}$, where N is the polymer chain length and σ_g is the grafting density. In the intermediate regime of surface coverage, all of the counterions become condensed inside the chain. In this "osmotic regime," the osmotic pressure of the ions is the dominant effect, and the brush stays stretched regardless of the grafting density. There is no dependence on grafting density. If the charge density is lowered, the brush enters the "Pincus" regime. Here, the height of the brush depends linearly on the grafting density. In the Pincus regime the counterions extend beyond the brush, and the osmotic pressure of the counterions is not sufficient to overwhelm the repulsive forces between monomers arising from electrostatic interactions. Csajka *et al.*[24] put forth an extended scaling theory that considers the effects of electrostatic correlations that may cause attractions. This theory predicts the existence of a "collapsed" regime if electrostatic coupling is high, requiring that the Gouy-Champman length be much less than the brush height. In some respects, the quasineutral and collapsed regimes are similar, with both showing increasing brush height with increasing grafting density. In this work we study whether these regimes are observed for short chain lengths.

There are experimental studies of flexible polyelectrolytes end tethered to a single hard wall[25–31] and polyelectrolytes at interfaces, such as an air/water interface.[32–36] The surface force apparatus has been used in several studies[37–41] to measure the force experienced by bringing two polymer brushes attached to mica walls together. Though the most commonly studied strong polyelectrolyte is sodium polystyrene sulfonate (NaPSS), biopolymer systems[39] such as grafted polysaccharides and self-assembled monolayers,[3] modified to bear electric charge, are also of interest for biological and sensor applications. Hayashi *et al.*[39] have examined systems of grafted poly(*L*-glutamic acid) and poly(*L*-lysine) in water using the surface force apparatus. Raviv *et al.*[37] have demonstrated the outstanding lubrication properties of grafted polyelectrolytes by studying a block copolymer with a long hydrophilic sodium sulphonated glycidyl methacrylate block. The measurements of the interactions using the surface force apparatus provide only indirect information on the structure of the layer.

Tran and Auroy[25] and Tran *et al.*[29] observed that grafted NaPSS chains are strongly stretched in salt-free water because of the strong electrostatic repulsion between the unshielded, like-charged monomers. They found that the brush thickness is proportional to the chain length, but they found no dependence on the grafting density, consistent with the osmotic regime. However, others[33] found increasing height with increasing grafting density. Generally, the experiments support the conclusions of Csajka *et al.*,[24] reached using the scaling theory and molecular dynamics simulations. The brush height scales linearly with the length of the polyelectrolyte chains, and the brush height is independent of the grafting density in the strongly charged regime.

Molecular dynamics (MD) and Monte Carlo (MC) simulations are well suited to examining the predictions of scaling theories and exposing the underlying physics behind experimental observations. MD is the principal simulation tool used thus far to study polyelectrolyte brushes. Csajka and Seidel[42,43] have studied end-grafted polyelectrolyte systems using a bead-spring model. For strongly charged systems they observed a chain collapse,[42] while at moderate charge strength Seidel[44,45] predicted that brush height depends weakly on the grafting density, indicative of the osmotic regime.

MC simulations for polyelectrolyte brushes have been less numerous than MD simulations. Chen *et al.*[46] used a lattice MC simulation to examine polyelectrolyte brushes, treating electrostatic interactions with a screened Coulombic potential. Counterions were not treated explicitly, and excluded volume interactions were ignored. In the strongly condensed regime the charged brush behaved similarly to a neutral brush. In the weakly screened regime the scaling behavior for the brush height followed that of the Pincus regime, as expected. MC simulations have also been used to study untethered polyelectrolyte chains.[47,48]

The molecular theory (MT) utilized in this study is an extension of the single-chain mean-field theory used for neutral brushes[11] and recently extended to include electrostatic interactions.[49,50] The theory explicitly accounts for the conformations of the chains, and it includes the size, shape, and charge distribution of each molecular species in the system. The theory has been applied to the study of adsorption of charged proteins on surfaces with and without grafted polymers.[49–51] The theory has been extended to study weak polyelectrolytes grafted on surfaces of various geometries.[52] The predictions of the theory for end-grafted polyelectrolytes are in excellent quantitative agreement with experimental observations for the height of polyacrylic acid layers as a function of surface coverage, *p*H, and salt concentration.[54,55] In the work presented here we extend the theory to include counterion condensation. The comparison of the predictions of the theory with the MC simulations is the most stringent test for the molecular approach because MC provides for the exact solution of the identical model system used in the theory. Moreover, we study the cases where there is no added salt, and thus electrostatic interactions are not screened. As it will be shown, the predictions of the theory are in very good agreement with the simulation results, supporting the assumption that the approximations used in the derivation of the theory are valid and that the MT can be used as a quantitative tool, when full scale simulations are too expensive to be carried out.

In this work, randomly grafted polyelectrolytes on a single charged wall are examined using MC simulations. Counterions are included explicitly and electrostatics are treated exactly through Ewald summation, not through the Poisson-Boltzmann approximation. Rosenbluth biasing, a

Downloaded 28 Jun 2007 to 128.220.135.141. Redistribution subject to AIP license or copyright, see http://jcp.aip.org/jcp/copyright.jsp

novel distance biasing scheme, and the use of a lattice are all used to speed up calculation, enabling MC simulation to effectively simulate this complex system in a reasonable amount of computer time. The effect of grafting density, surface charge density, charge strength, and polymer chain length are studied. A comparison to MT calculations for the same model system are made, allowing a direct evaluation of the validity range of the theory.

In the next section we present the model system followed by the details of the MC simulations. Following that, we present a short derivation of the molecular theory with an emphasis on the novel features, namely, the inclusion of counterion condensation in the theory. Section III presents the results of the calculations using both methods, followed by some concluding remarks and directions for future work.

II. MODEL AND METHODS

A. Model

The model system studied represents flexible polyelectrolytes tethered to a hard wall. The polymer is modeled as a chain of N coarse-grained beads occupying consecutive sites on a simple cubic lattice having a coordination number of $Z=26$, with allowed lattice vectors of (0, 0, 1), (0, 1, 1), and (1, 1, 1), and their reflections. Each counterion bead also occupies a single lattice site. Lattice spacing is a. The solvent molecules are not included explicitly since they are represented by the empty lattice sites. The polymer beads, all of which carry a single negative charge, and the counterions, all of which carry a single positive charge, interact with each other through Coulombic and excluded volume interactions. A snapshot of the model system is shown in Fig. 1.

The dimensionless temperature is defined as

$$T^* = \frac{4\pi\varepsilon\varepsilon_0 a k_b T}{e^2} = \frac{a}{l_B}, \tag{1}$$

where l_B is the Bjerrum length and is 7.14 Å in water ($\varepsilon=78.5$) at room temperature ($T=298$ K). The inverse of this dimensionless temperature defines the dimensionless Manning ratio,

$$\xi = \frac{1}{T^*} = \frac{l_B}{a}. \tag{2}$$

The dimensionless Manning ratio relates the strength of the electrostatic interaction to the distance between the charges.

The grafting density is defined as

$$\sigma_g = \frac{N_g}{L_x L_y}. \tag{3}$$

Grafting densities from 0.01 to 0.08 are examined in this work. Images of the grafted polymer surface produced in two atomic force microscopy studies[30,41] show clusters of grafted polyelectrolytes, but another study[2] shows seemingly random grafting. Exactly what grafting pattern predominates remains unclear. This study adopts random grafting. Previous work has examined a fixed triangular lattice pattern.[56]

Though none of the experiments[25–41] measured the magnitude of the charge on the silica walls, it is known that Si forms Si–OH groups with a density dependent on the pH of the aqueous solvent. Typically, a silica surface might have 2–12 hydroxyl groups per nm^2.[57] For example, if $a=3.6$ Å and the simulated charged wall is $10a$ per side, this corresponds to approximately $25e$ to $150e$ of negative charge on the wall. The surface charge fraction is defined as

$$\sigma_\pm = \frac{Q_{\text{wall}}}{eL_xL_y}, \tag{4}$$

where Q_{wall} is the total charge on the wall and e is the charge on one electron. This study examines surface charge fractions in the range of $-0.8 \leqslant \sigma_\pm \leqslant +0.2$, a range consistent with experimental observations.

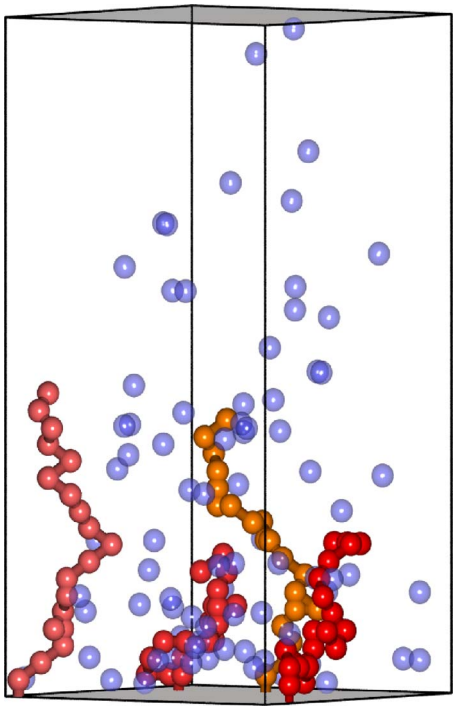

FIG. 1. (Color online) Snapshot of Monte Carlo simulation of a system with $\xi^*=0.2$, $L_z=40$, $\sigma_g=0.01$, and $N=20$. Polyelectrolytes that span the periodic boundaries are shown intact for visual clarity. Counterions are shown as transparent blue (light) beads and polymer chains as different shades of solid red (dark) beads. Top and bottom walls are shaded to indicate that they are not subject to periodic boundary conditions.

B. Monte Carlo simulations

In our canonical (NVT) ensemble Monte Carlo simulations, the polymer configurations are sampled using a Rosenbluth-biased chain regrowth procedure, while the associated counterion positions are sampled using a standard displacement algorithm. The MC simulation proceeds by randomly attempting counterion displacement and chain regrowth moves. Chain regrowth is attempted 10%–80% of the time, and counterion displacement the remainder. The percentage of chain regrowth moves attempted is adjusted so that, on average, all counterions are displaced many times between successful chain regrowth moves.

The regrowth of a polyelectrolyte chain in the strongly charged regime has an unacceptably low acceptance rate unless biasing schemes are utilized. In particular, Rosenbluth

Downloaded 28 Jun 2007 to 128.220.135.141. Redistribution subject to AIP license or copyright, see http://jcp.aip.org/jcp/copyright.jsp

biasing[58] is required to sample favorable chain configurations. Under a certain limited range of strong charge and high grafting density, distance biasing is also useful to find preferable arrangements of each chain's counterions. We adopt the distance bias method utilized by Orkoulas and Panagiotopoulos[59] and later by Hynninen *et al.*[60] for cluster moves of a charged ion and its counterions. We modify the method for the canonical ensemble, polymer chains, and complications due to a finite geometry. Finiteness increases the computational times required for electrostatic summation. The distance bias scheme of Hynninen *et al.* increases in complexity in a finite geometry because sums over the volume become z dependent. The supplemental material[61] provides more details on how finiteness requires alterations to standard methodologies. The proof of a detailed balance for this regrowth move is also provided as a supplemental material.[61] It was found that this distance bias method was not substantially better than Rosenbluth bias alone in this particular lattice system. Here, we summarize only the general approach of the method.

When a charged monovalent monomer is to be removed, its counterion i is selected for removal with probability

$$P_i = \frac{\omega(r_i)}{\sum_{j=1}^{N_c} \omega(r_j)}, \tag{5}$$

where

$$\omega(r_j) = \exp[-\beta Q_b U(r_j)]. \tag{6}$$

r_j is the distance between the counterion to be removed and the monomer bead, N_c is the total number of counterions, and Q_b is a free parameter used to vary the strength of the distance bias. The removal of all counterions for a chain is given by the product of the individual removal probabilities,

$$P = \prod_{i}^{N_c} P_i. \tag{7}$$

The Rosenbluth factor of the removed chain, P_r^{old}, is also calculated.

As Q_b is increased, the rate of decay of the probability distribution function as a function of distance increases. An examination of the acceptance rates shows that the optimal Q_b varies greatly with density and temperature, but is typically in the range $0 \leqslant Q_b \leqslant 10$. Generally, the optimal Q_b was larger for high charge density systems than for low density systems. An important consistency test for any distance bias algorithm is that statistically identical results are produced, regardless of the value of Q_b. Our simulation algorithm exhibits the required consistency, and the results are invariant with the value of Q_b.

The reverse event, the growth of a chain and placement counterions, is similar. A complete chain cut and regrowth move is accepted with probability

$$P = \min\left(1, \frac{P_r^{\text{new}}}{P_r^{\text{old}}} \frac{P^{\text{new}}}{P^{\text{old}}} \exp[-\beta \Delta U]\right), \tag{8}$$

where P^{new} denotes the probability of counterion insertion in the new (attempted) state, P^{old} the probability in the old (current) state, P_r the Rosenbluth factors, and ΔU the difference in electrostatic energy between the old and new states.

We have used the method of Heyes *et al.*[62] to do summation of the electrostatic energy. This particular method is not the fastest known, as it scales as N^2 with the number of particles, compared with the recent MMM2D method of Arnold and Holm,[63] which scales as $N^{5/3}$ with the number of particles. However, because of the lattice geometry, the Ewald sum may be precomputed once at the beginning of the simulation,[64] and not at every simulation step.

C. Molecular theory

The basic idea of the MT is to to treat each molecular species exactly, namely, considering the intramolecular and surface interactions exactly while the intermolecular interactions are treated in an approximate way. This is true for nonelectrostatic interactions. The electrostatic interactions are obtained by the inclusion of the charge distribution of each polymer conformation, the explicit inclusion of counterions and their charges, and the consideration of the possibility of counterion condensation on the polymer chain. The electrostatic potential is determined by coupling the electrostatic and packing interactions through the minimization of the total free energy functional. The end result is a theory that is much more general than the commonly used Poisson-Boltzmann approach since the MT explicitly includes the size, shape, conformations, and charge distribution of all the molecular species as derived next. For a complete derivation of the theory (without counterion condensation) and the approximations involved, the reader is referred to Ref. 52.

We consider exactly the same system as that treated in the simulations, namely, N_g grafted polyelectrolyte molecules with N segments each on a planar surface ($z=0$) with a total surface area A. The grafting density (surface coverage) is then given by $\sigma_g = N_g/A$. The surface may be either charged with a surface charge density $\sigma_{\pm}$ or neutral. Each of the N segments is charged as in the simulated system. The polyelectrolyte layer is in contact with a solution containing counterions and solvent. No salt ions are assumed to be present. Since the whole system is assumed to be electroneutral, the charges on the surface and polymer brushes are exactly counterbalanced by the counterions in the solution. Each polymer bead, as well as each counterion, occupies a single lattice site. The remaining space is filled by the solvent molecules, which also occupy a single lattice site. The interactions considered are identical to the simulated system, i.e., electrostatic interactions between the charged species and excluded volume interactions between all the molecular species, which translates to single occupancy for each lattice site.

The first step in the derivation of the theory is writing the free energy density (per unit area), F/A, as a functional of the density of counterions, density of solvent, the probability distribution function (pdf) of the chain conformations, and the electrostatic potential. We write all the expressions in continuum space since the approach is applicable to any type of molecular description, as shown for realistic chain models in Refs. 52 and 54. We then discretize the equations for a lattice, to be applied to the system of interest here, i.e., the

Downloaded 28 Jun 2007 to 128.220.135.141. Redistribution subject to AIP license or copyright, see http://jcp.aip.org/jcp/copyright.jsp

simulated systems. Furthermore, we assume that the system is inhomogeneous only in the direction perpendicular to the surface. This assumption is justified *a posteriori* by the very good agreement between the theoretical predictions and the MC results. For the consideration of inhomogeneities in more than one direction, see Refs. 52 and 65.

The free energy functional is given by

$$\frac{\beta F}{A} = \sigma \sum_{\alpha} P(\alpha) \ln P(\alpha) + \int \rho_s(z)(\ln \rho_s(z) - 1) dz + \int \rho_+(z)(\ln \rho_+(z) v_s - 1) dz + \int \sigma(n_p(z)) \{ f(z) \times [\ln f(z)] + (1 - f(z))[\ln(1 - f(z)) + \beta \Delta \mu_{AP}^0] \} dz + \beta \int dz [\langle \rho_q(z) \rangle \psi(z) - \frac{1}{2} \epsilon (\nabla_z \psi(z))^2]. \quad (9)$$

The first term is the conformational entropy of the grafted polymers. The second and third terms correspond to the mixing (translation) entropy of the solvent and counterions, respectively. v_s is the volume of a solvent molecule, which in the case treated here is the same as the volume of a polymer segment (v_p) and that of the counterion (v_+). The next integral in Eq. (9) includes the mixing and free energy terms related to counterion binding, where $\langle n(z) \rangle$ denotes the average number of polymer segments per chain at distance z from the surface, $f(z)$ represents the fraction of polymer segments at z that are charged, and thus $(1-f(z))$ is the fraction that have counterions bound to them. $\Delta(\mu_{AP}^0)$ is the difference in standard free energy between two charged units separated by an infinite distance and the bound counterion on the polymer segment. The last two terms in the free energy expression [Eq. (9)] are the electrostatic contribution, with $\langle \rho_q(z) \rangle$ representing the total charge density at z given by

$$\langle \rho_g(z) \rangle = -\sigma f(z) \langle n(z) \rangle + \rho_p(z), \quad (10)$$

where the negative charge in the polymer and the positive in the counterion has been accounted for. In Eq. (9) $\psi(z)$ is the electrostatic potential at z. ϵ is the dielectric constant of the medium (for the case of varying dielectric environment see Ref. 52).

The single occupancy requirement, hard core excluded volume interactions, is introduced through packing constraints. Namely, at each distance from the surface the available sites are occupied by polymer segments, solvent, or counterions. This reads

$$\sigma \langle n(z) \rangle [f(z) v_p + (1 - f(z))(v_p + v_+)] + \rho_+(z) v_+ + \rho_s(z) v_s = 1. \quad (11)$$

The first term is the contribution from the polymer segments. There are two types of polymer segments that need to be considered: those that are charged and the ones that have a counterion condensed. Note that in considering two types of polymer segments, we are also considering two types of counterions, condensed and free. This has also been done in the free energy as $\rho_+(z)$ is the density distribution of *free* counterions. The second term in the constraint equation [Eq. (11)] includes the contribution from the free counterions, and the last term is the solvent contribution.

The pdf, the density of solvent and counterions, the fraction of bound counterions, and the electrostatic potential are determined by the functional minimization of the free energy [Eq. (9)] subject to the packing constraints [Eq. (11)] with an explicit consideration of the charge distribution [Eq. (10)]. This is done by the introduction of Lagrange multipliers $\beta\pi(z)$ to yield, after some algebraic rearrangement[52] for the pdf,

$$P(\alpha) = \frac{1}{q} \exp\left[- \int \beta \pi(z) n(z;\alpha) - \int [\psi(z) - \ln f(z)] n(z;\alpha) dz \right], \quad (12)$$

where q is the normalization constant. The first term in the exponential represents the (nonelectrostatic) repulsive interactions that the polymer in conformation α feels, and the last one is the electrostatic contribution with the explicit inclusion of the role of counterion condensation.

For the density of free counterions the free energy minimization leads to

$$\rho_+(z) = C \exp[-\beta \pi(z) v_p - \beta \psi(z)], \quad (13)$$

where the constant C is determined by the condition that the total number of counterions is equal to the total number of polymer segments (recall that we are treating only the salt-free case, as that is the case treated in the MC simulations).

The solvent density profile is

$$\rho_s(z) v_s = \exp[-\beta \pi(z) v_s], \quad (14)$$

and the fraction of charged polymer segments at z obtained from the minimization (and some algebraic rearrangements) is

$$f(z) = \frac{1}{1 + \rho_+(z) \exp[-\beta \Delta \mu_{AC}^0]}. \quad (15)$$

Finally, the minimization of the free energy functional [Eq. (9)] with respect to the electrostatic potential leads to

$$\frac{\partial^2 \Psi(z)}{\partial z^2} = -l_B \langle \rho_q(z) \rangle, \quad (16)$$

with the average charge at z given by Eq. (10).

Equation (16) demonstrates that the molecular theory presented here goes well beyond the Poisson-Boltzmann equation since the average of the charge density explicitly includes the conformations of the polymer chains, the size and shape of each of the molecular species, as well as the specific condensation equilibrium. A thorough discussion of the advantages of the theory, its range of application, the physical significance of all the terms, as well as the limitations of the approach can be found in Ref. 52.

The next step is the application of the derived equations to the systems of interest here. The only unknowns to calculate any desired conformation or thermodynamic property of the polymer layer are the lateral pressures and the electrostatic potential as a function of the distance from the surface.

Downloaded 28 Jun 2007 to 128.220.135.141. Redistribution subject to AIP license or copyright, see http://jcp.aip.org/jcp/copyright.jsp

Since we are only interested in the case of lattice chains in the present application, we discretize the above derived equations directly for a lattice in which the lattice step size as well as the lattice site volume are taken as unity (for the application of the theory to off-lattice systems, including mixtures of molecules of different sizes, shapes, and charge distributions, see Refs. 49, 51, 52, and 66). Then, the explicit equations to be solved are the coupled constraint [Eq. (11)] and the generalized Poisson equation [Eq. (16)], in the lattice, which are

$$\sigma\langle n(i)\rangle + \rho_+(i) + \rho_s(i) = 1, \quad i = 1, \ldots, L_z \tag{17}$$

and

$$\Delta^2\Psi'(i) = -\frac{l_B}{a}\langle\rho_q(i)\rangle = \xi\langle\rho_q(i)\rangle, \quad i = 1, \ldots, L_z, \tag{18}$$

where Δ^2 is the second difference operator defined by $\Delta^2 g(i) = g(i+1) - 2g(i) + g(i-1)$. The pdf in lattice form is given by

$$P(\alpha) = \frac{1}{q}\exp\left[-\sum_{i=1}^{L_z}\{-\pi'(i) - \Psi'(i) - \ln f(i)\}n(i;\alpha)\right], \tag{19}$$

while the solvent density is given by

$$\rho_s(i) = \exp[-\pi'(i)] \tag{20}$$

and the counterion density is

$$\rho_+(i) = C\exp[-\pi'(i) - \Psi'(i)], \tag{21}$$

where the lateral pressures $\pi'(i)$ and the electrostatic potential $\Psi'(i)$ in Eqs. (18)–(21) are unitless quantities, defined by $\pi'(i) = \beta\pi(i)v_s$ and $\Psi'(i) = \beta\Psi(i)e$.

The Poisson equation requires the specification of two boundary conditions. In order to have the same system as in the simulations, the boundary conditions should be that the charge at the grafted surface, $i=0$, is $\sigma_\pm$ while the charge at the surface L_z should be equal to zero. The charge is given by the gradient of the electrostatic potential. Thus, the boundary conditions for the lattice system are

$$\Psi'(1) - \Psi'(0) = \xi\sigma_\pm \text{ and } \Psi'(L_z+1) - \Psi'(L_z) = 0. \tag{22}$$

Note that the way the differences are defined, the derivatives are calculated exactly at the surfaces. Moreover, it should be clear that there are no layers 0 and L_z+1, but they are needed to define the derivatives.

Equations (17) and (18) represent a set of coupled $2L_z$ nonlinear equations to determine the complete set of values for $\pi'(i)$ and $\Psi'(i)$. The input necessary to solve the equations are the polymer surface coverage, the surface charge density, the value for the standard free energy for ion condensation, and the set of polymer conformations. To this end, depending on the chain length, we can generate all the possible self-avoiding configuration by exhaustive counting for short chain length or generate a large set of self-avoiding walks using the Rosenbluth-Rosenbluth algorithm. Note that for a given chain length the set of conformations is generated once, and then the same set is used for all the different conditions. From each generated polymer conformation the set of occupation numbers is used. The set of nonlinear equations is solved by standard numerical methods.

The value of $\Delta\mu_{AC}^0$ is the difference between the free and bound counterion states. In the bound state most of the polymer conformation will be such that the counterion can be in contact with more than one polymer segment. The only type of polymer configurations in which there is only one contact is that where two consecutive bonds are linear. Therefore, the free energy value should be $\beta\Delta\mu_{AC}^0 = C\xi$, with $C>1$. We have taken the value $C=1.5$ in all the calculations.

III. RESULTS AND DISCUSSION

Results have been obtained using MC calculations and MT theory for polymer chains of length $N=10$ and 20 at grafting densities of $\sigma_g=0.01$, 0.04, and 0.08. The charge on the grafting surface, $\sigma_\pm$, ranged from $\sigma_\pm=+0.2$ to $\sigma_\pm=-0.8$.

Regardless of chain length, all monomer density profiles found using MT theory and MC simulation exhibit an entropic depletion near the wall, a peak in the monomer density profile adjacent to the region of depletion, and a gradual decay, as has been seen in previous mean-field calculations[22] as well as in Monte Carlo simulations[46] for much longer chains.

In the limit of $\xi\to 0$ the electrostatic interactions disappear and the counterions distribute evenly across the entire gap, with some deviation due to excluded volume interactions with the polyelectrolyte chains. Counterion condensation within the polymer brush is promoted by increasing ξ. At $\xi>1$ the electrostatic interactions become strong enough for the counterions to condense immediately adjacent to the negative charges on the chains, effectively neutralizing the chain. Therefore, the polyelectrolyte layer behaves similarly to neutral tethered polymers. Figure 2 illustrates the behavior of low surface coverage tethered polyelectrolytes ($\sigma_g=0.01$) between the two limits. At a charge strength of $\xi=0.2$ [Fig. 2(a)] the counterions are spread across the gap of width $L_z=40$. There is a slight tendency to have an enhanced counterion density close to the polymer due to the weak electrostatic attractions. As the Manning parameter increases from $\xi=0.2$ to $\xi=1$ [Fig. 2(b)], the monomer density in the first few layers drops and the density of the counterions in these layers rises, showing the more dominant role of electrostatic interactions. Interestingly, from the density profiles it is not clear whether the counterions are condensed or freely attracted to the polymer layer region due to electrostatic attractions between the oppositely charged groups. The inset of each curve shows the free and bound counterion densities as predicted from the theory. At small ξ there are almost no condensed ions. However, for $\xi=1$ there is a significant amount of condensed ions, as would be expected.

At $\xi=4$ [Fig. 2(c)] the condensation is so strong (see inset) that the density profile of the counterions is almost coincident with the monomer density profile. At $\xi=4$ the polymer layer is less stretched and the behavior is very similar to that of an uncharged tethered polymer layer. Csajka and Seidel[42] also observed a decreased brush extension in their simulations. Their simulations[43] were completed at $\xi=14$, a region of extremely strong counterion condensation.

Downloaded 28 Jun 2007 to 128.220.135.141. Redistribution subject to AIP license or copyright, see http://jcp.aip.org/jcp/copyright.jsp

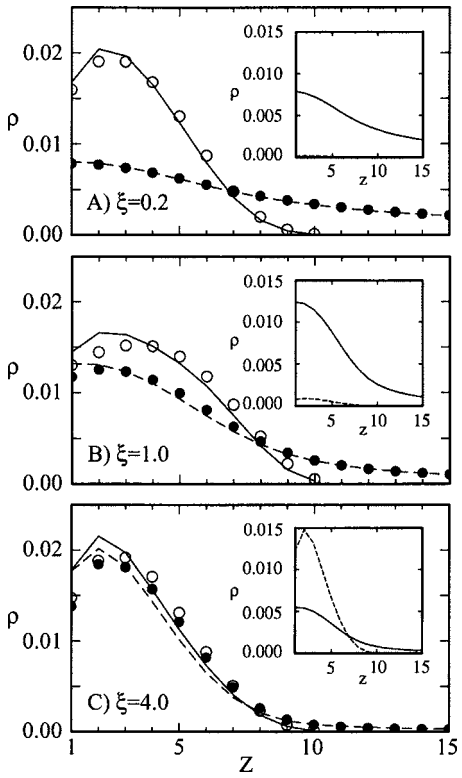

FIG. 2. Monomer density (solid line) and counterion density (dashed line) profiles calculated using the mean-field theory. Monomer density (circles) and counterion density (filled circles) profiles calculated with the Monte Carlo simulation. Profiles at (A) $\xi=0.2$, (B) $\xi=1.0$, and (C) $\xi=4.0$ for $\sigma_g=0.01$, $N=10$, and $L_z=40$. Statistical uncertainties are smaller than the symbol size. Insets show free (solid) and condensed (dashed) counterion density profiles.

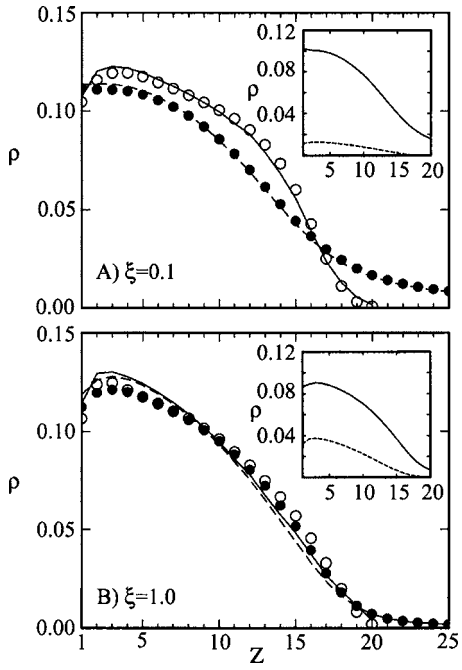

FIG. 3. Monomer density (solid line) and counterion density (dashed line) profiles calculated using the mean-field theory. Monomer density (circles) and counterion density (filled circles) profiles calculated with the Monte Carlo simulation. Profiles at (A) $\xi=0.1$ and (B) $\xi=1.0$ for $\sigma_g=0.08$, $N=20$, and $L_z=40$. Statistical uncertainties are smaller than the symbol size. Insets show free (solid) and condensed (dashed) counterion density profiles.

Our results are in agreement with their predictions, and even the short chains shown here can be considered to be in the quasineutral or collapsed regimes.

It is important at this point to emphasize that the results shown in Fig. 2 correspond to a very low surface coverage of polymers. Actually, in the terms typically used to characterize neutral tethered polymers, this is the mushroom regime, in which the distance between grafting points is larger than the radius of gyration of the neutral polymer chain. The study of this regime is important for several reasons. First, in experimental systems such as cell membranes, short polysaccharides are found on the outer leaflet of the membrane at low surface coverages. Second, the complete understanding of the behavior of the grafted chains requires the study of all the limits from low to high density. Third, from the point of view of the molecular theory this is the most stringent test for polyelectrolytes. The reason is that in neutral chains the molecular theory and the simulations are identical at very low surface coverages since the theory exactly accounts for the single-chain properties. However, the addition of electrostatic interactions makes the low density limit the most challenging for the theory. The fact that there is a close agreement between the MT predictions and the simulations for the three values of ξ (for both the polymer segments and the counterion distribution) implies that the electrostatic interactions, with the inclusion of counterion binding, are well accounted for by the theory. The main difference between the theoretical predictions and the simulations are for large ξ and only in the region very near to the surface.

The predictions of the theory are also in very good agreement with the MC simulations for a longer chain length and at high grafting density, as shown in Fig. 3. The figure shows that for large values of σ_g there is a larger degree of counterion condensation in order to reduce the electrostatic repulsions induced by the high local density of polymer segments. Even for a low value of ξ we observe a large concentration of the counterions in the region of the polymer layer. The entropic gain of spreading the ions, as observed in Fig. 2(a), is overcome by the gain in electrostatic attraction or, equivalently, the reduction in the interpolymer electrostatic repulsions. Again, the comparison with the theoretical predictions demonstrates the validity of the approach for all conditions of surface and chain length studied here.

A measure of the thickness of the polymer layer is given by the height, which can be calculated as the first moment of the density profile,

$$h = \frac{1}{\sigma_g N} \sum_{i=1}^{N} z_i \rho_i. \tag{23}$$

Figure 4 illustrates the interplay between electrostatic interactions and elastic free energy. The height of the layer shows a maximum as a function of the Manning parameter. At low Manning parameters the electrostatic interactions are very small due to the large distance (as compared to the Bjerrum length) between charges. Therefore, the height reflects the stretching of the chains due to the elastic free energy of the chains. As the Manning parameter increases, the

Downloaded 28 Jun 2007 to 128.220.135.141. Redistribution subject to AIP license or copyright, see http://jcp.aip.org/jcp/copyright.jsp

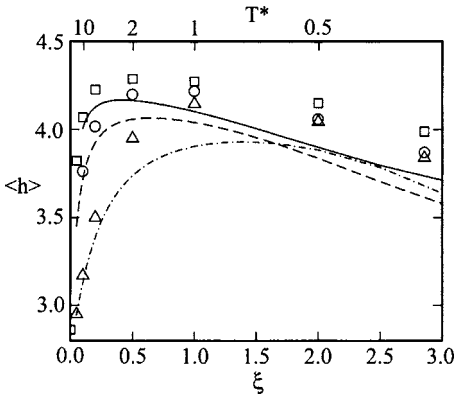

FIG. 4. Brush height as a function of the Manning parameter calculated using the mean-field (MF) theory (lines) and MC simulation (symbols) for grafting densities of $\sigma_g=0.01$ (dash-dot/triangles), 0.04 (dashed/circles), and 0.08 (solid/squares) for $N=10$ and $L_z=40$. Statistical uncertainties are comparable to the symbol size and tabulated in Ref. 61.

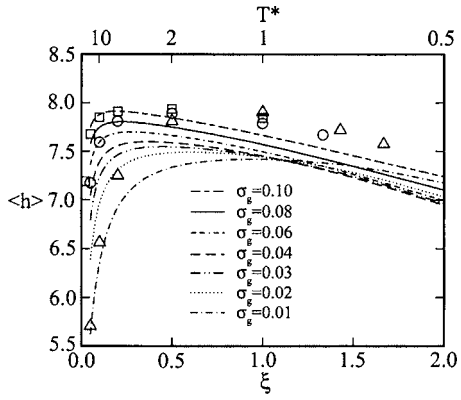

FIG. 5. Brush height as a function of the Manning parameter calculated using the MF theory (lines) and MC simulation (symbols) for grafting densities of $\sigma_g=0.01$ (triangles), 0.02, 0.03, 0.04 (circles), 0.06, 0.08 (squares), and 0.10 for $N=20$ and $L_z=40$. The line type denoting the molecular theory results is indicated within the figure. Statistical uncertainties are comparable to the symbol size and tabulated in Ref. 61.

electrostatic repulsions start playing a more important role and there is an enhancement of the stretching of the chains due to the charge-charge repulsions. However, when the electrostatic interactions start to become very dominant, the system has the option of condensing some of the counterions, resulting in an effective smaller charge on the chain and thus a decrease in the film thickness. The height results are clearly a manifestation of the changes in the detailed profiles shown in Figs. 2 and 3. The presentation of the height variations provides a more concise way to show the variations scanning a larger parameter space, enabling the analysis of different surface coverages within one picture.

Figure 4 shows the predictions from the MC and those from the MT. There is good agreement at all surface coverages for all values of the Manning parameter. The best agreement though is found at higher surface coverages. However, in all the calculations that we have carried out for $N=10$ and $N=20$, we find the maximal error in the predictions from the theory as compared to the MC to be 6.4% for $\sigma_g=0.01$ and 3.5% for $\sigma_g=0.08$. Taking these results with the comparisons shown for the density profiles in Figs. 2 and 3, we can be confident in the predictions of the theory as it quantitatively predicts the detailed structure of the layer within less (sometimes much smaller) than 5% error in most cases of interest.

The examination of Fig. 4 shows that the variation of the height with the strength of the electrostatic interactions is not the same for all grafting densities. To see this effect in a clearer way, Fig. 5 displays the predictions from the MT for $N=20$ at seven different surface coverages, ranging from low to very high. Also included in the figure are the MC results for three surface coverages. The shape of the variation of the height is the same for all σ_g, namely, the presence of the maximum. However, as the curves are almost parallel in the limit of low ξ, this is not the case for $\xi \gtrsim 1$. We see that both the position of the maximum as well as the decrease as ξ increases are density dependent, with the strongest dependence at low surface coverages. The reason for this behavior can be understood by looking at the different roles of the electrostatic and the steric interactions in determining the structure of the layer. For low surface coverages, the electrostatic contributions are the most dominant interaction, and the intermolecular repulsions between charged groups are responsible for most of the behavior observed for $\sigma_g=0.01$. For high surface coverages, the steric intermolecular repulsion is mostly responsible for the stretching of the chains, and both intra- and intermolecular electrostatic repulsions play a more important role. As the steric repulsions are more dominant in stretching the chains (as σ_g increases), the maximum in the height of the tethered layers moves towards lower values of ξ. The position of the maximal height at lower ξ demonstrates that there are more counterions, both condensed and free, in the region of the polymer at lower ξ as σ_g increases. This is the result of the more dominant role of *intermolecular* electrostatic repulsions.

The chain lengths described in this work are relatively short, and therefore scaling theories that are valid in the limit of very long chains are not applicable. However, it is interesting to comment that even for these short chain lengths we start to see the predicted behavior for long chain lengths. For example, at $\xi \simeq 1$ we see that there is a very weak dependence of the height on surface coverage. In the scaling limit $\xi=1$ represents the osmotic regime, where the thickness is predicted to be independent of surface coverage.[19] We can also see that the height increases monotonically with σ_q at low ξ, while it shows a minimum for $\xi>1$, with the position of the minimum being a function of ξ.

The quantification of counterion condensation is difficult within the MC simulations due to the way that chains are generated and regenerated constantly. However, based on the high quality of the predictions of the theory as judged against the simulations, we are confident that the theoretical predictions for other quantities not defined in the simulation are accurate as well. Therefore, we use the predictions of the theory to show the amount of counterion condensation as a function of the Manning parameter in Fig. 6. The counterion condensation is defined as the fraction of the ions that form pairs with the polymer chain (see insets in Fig. 2). Because we calculate the counterion condensation only for systems where the charged chains are exactly counterbalanced by the

Downloaded 28 Jun 2007 to 128.220.135.141. Redistribution subject to AIP license or copyright, see http://jcp.aip.org/jcp/copyright.jsp

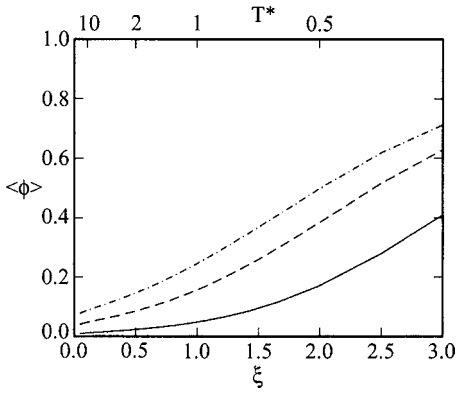

FIG. 6. The counterion condensation fraction ϕ vs the Manning parameter ξ calculated using the mean-field theory for σ_g=0.01 (dash-dot), 0.04 (dash), and 0.08 (solid) for N=20 and L_z=40.

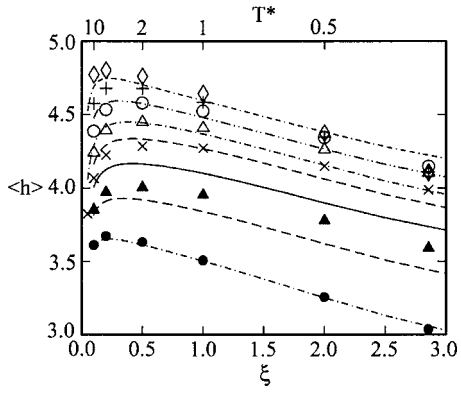

FIG. 7. Brush height as a function of the Manning parameter calculated using MT (lines) and MC simulation (symbols) for surface charges of $\sigma_\pm$ =+0.2 (dot-dash/filled circle), +0.1 (dashed/filled triangle), 0 (solid line/cross), −0.1 (dashed/triangle), −0.2 (dot-dash/circle), −0.4 (dot-dot-dash/plus), and −0.8 (dash-dash-dot/diamond) for N=10, σ_g=0.08, and L_z=40. Statistical uncertainties are smaller than the symbol size.

oppositely charged counterions, the counterion condensation fraction may be calculated from the the fraction of polymer segments that are charged, and is given by

$$\langle \phi \rangle = \frac{1}{N} \sum_{i=1}^{L_z} (1 - f(i)) \langle n(i) \rangle, \tag{24}$$

with the quantities as defined in Sec. II.

The counterion condensation $\langle \phi \rangle$ as a function of the Manning parameter is shown in Fig. 6. As already discussed above, there is a sharp increase in the condensation of the counterions as ξ increases. Interestingly, we also see a strong dependence of the counterion condensation on surface coverage. In order to reduce the overall electrostatic repulsions, a larger fraction of the polymer segments need to have the counterions bound as the surface coverage increases. This, as discussed above, is a direct manifestation of the role of intermolecular interactions as the surface coverage increases.

Consider now the case in which the grafting surface is charged. If the wall and the polyelectrolyte are like charged (a typical polyelectrolyte and silica wall system in water), the electrostatic repulsions would induce the stretching of the polymer chains, as compared to an uncharged wall. This effect is predicted using both MC and MT calculations. As in all the cases above, there is very good agreement between the predictions of the theory and the simulations, with less than 5% difference in the worst case. The increased polymer layer extension with surface charge is observed for the entire range of ξ examined, as shown in Fig. 7. For a layer with a total charge of $-80e$ at ξ=0.5, as the total negative charge on the wall rises from zero to $-80e$ ($\sigma_\pm$=−0.8), the polymer layer height increases by 11%. An increase in height was also predicted by Borisov *et al.*[22] using a mean-field theory. If the wall and the polyelectrolytes are oppositely charged, the change in layer thickness is larger in magnitude than observed in the like-charged case. Figure 7 shows that in a system where the total layer charge is $-80e$ and the wall charge is $+20e$, the polymer thickness decreases from 4.29 to about 3.63 (at ξ=0.5), a 15% decrease. However, if the wall charge is $-20e$ instead the brush increases in height by only 7%.

IV. CONCLUSIONS

We have examined the structure of grafted polyelectrolyte layers as a function of charge strength, grafting density, surface charge, and chain length using both Monte Carlo simulations and the molecular theory.

Monte Carlo simulations and the molecular theory both show that grafted polymer layers collapse at high charge strength due to counterion condensation. This effect is similar to the collapse in bulk solutions of highly charged chains to dense neutral structures, first predicted by Gonzalez-Mozuelos and Olvera de la Cruz,[53] due to the ionic correlations among condensed ions and the chains.

The layer thickness reaches a maximum at an intermediate ξ and falls as the Manning parameter decreases and the brush enters the weakly charged regime. The molecular theory agrees quantitatively with the MC results, with a better agreement at high grafting densities. It is important to emphasize that the theory requires the explicit inclusion of counterion condensation in order to predict quantitatively the properties of layers under all conditions. We have shown that counterion condensation can be treated in the theory as a chemical equilibrium between two different species, the bound pair and the separated charges. The free energy difference between the bound pair and the separate ions is an input for the theory. This type of chemical equilibrium has also been used within the same theoretical approach to treat acid-base equilibrium.[52] The predictions of the theory are in excellent quantitative agreement with experimental observations on polyacrylic acid grafted layers.[54,55] Thus, with the extension of the theory presented here, the molecular theory can be used in cases where both acid-base equilibrium and counterion condensation are possible.

We find that there is a weak dependence of layer height on grafting density at high ξ. Moreover, the film thickness shows a minimum as a function of surface coverage. At low ξ the thickness of the layer is a monotonic increasing function of the grafting density. This result is consistent with previous simulations[24] and scaling theory.[19] The simulations and theoretical predictions for charged surfaces show a mild

Downloaded 28 Jun 2007 to 128.220.135.141. Redistribution subject to AIP license or copyright, see http://jcp.aip.org/jcp/copyright.jsp

polymer extension for surfaces with the same charge as the polymer and a larger compression when the surface is oppositely charged.

The work presented here combines MC simulations with molecular theory. The aim of the work is to show the properties of short charged polymers end grafted to surfaces. While there is a relatively large body of work for long polymers, there is very little on short chain molecules. This range of chain length is important in biology, e.g., charged short sugars on membrane surfaces, and they may find important applications in the the design of charged self-assembled monolayers. We have shown that an efficient MC algorithm enables the systematic studies presented here for a variety of polymer grafting densities and charge strengths and for two chain lengths. However, this is still time consuming. The application of the molecular theory is orders of magnitude more efficient and can be used for realistic chains. The ability of the theory to quantitatively predict the properties of the layers, as compared with the MC, for all the conditions studied, strongly supports the validity of the approximations used in the derivation of the theory. The main approximation used in the theory is the neglect of lateral correlations, by assuming that at each z the layer is homogeneous. It is clear that in all the cases studied here, these correlations play almost no role in the determination of the properties of the layers. If lateral correlations are important, it implies that the theory implicitly includes this effect through the incorporation of counterion binding by a chemical equilibrium methodology. Note that the inclusion of the bound-unbound equilibrium is in essence a multibody effect.[67] The next step is to see whether this approximation is valid on more complex systems that include salt and the adsorption of charged nanoparticles on surfaces with grafted polymers. Work in this direction is being carried out.

ACKNOWLEDGMENTS

One of the authors (O.J.H.) acknowledges support from the Department of Energy through the Computational Sciences Graduate Foundation program, Grant No. DE-FG02-97ER25308. Two authors (A.Z.P. and O.J.H.) acknowledge financial support from the Department of Energy, Office of Basic Energy Sciences (Grant No. DE-FG02-01ER15121), with additional support from ACS-PRF (Grant No. 38165-AC9). The authors thank Professor Alexandre Diehl for assistance with the electrostatic summation implementation. Another author (I.S.) acknowledges financial support from The National Science Foundation through Grant Nos. NSF-CTS-0338377 and NSF-NIRT 0403903.

[1] P. V. Pavoor, B. P. Gearing, A. Bellare, and R. E. Cohen, Wear **256**, 1196 (2004).
[2] S. S. Balamurugan, G. B. Bantchev, Y. Yang, and R. L. McCarley, Angew. Chem., Int. Ed. **44**, 4872 (2005).
[3] J. Lahann, S. Mitragotri, T.-N. Tran, H. Kaido, J. Sundaram, I. S. Choi, S. Hoffer, G. A. Somorjai, and R. Langer, Science **299**, 371 (2003).
[4] R. R. Netz and D. Andelman, Phys. Rep. **380**, 1 (2003).
[5] J. Rühe, M. Ballauff, M. Biesalski *et al.* Adv. Polym. Sci. **165**, 79 (2004).
[6] A. V. Dobrynin and M. Rubinstein, Prog. Polym. Sci. **30**, 1049 (2005).
[7] P. G. DeGennes, *Scaling Concepts in Polymer Physics* (Cornell University, Ithaca, 1979).
[8] S. Alexander, J. Phys. (Paris) **38**, 983 (1977).
[9] P. G. DeGennes, Macromolecules **13**, 1069 (1980).
[10] S. T. Milner, T. A. Witten, and M. E. Cates, Macromolecules **21**, 2610 (1988).
[11] M. A. Carignano and I. Szleifer, J. Chem. Phys. **98**, 5006 (1993).
[12] T. Cosgrove, T. Heath, B. van Lent, F. Leermakers, and J. Scheutjens, Macromolecules **20**, 1692 (1987).
[13] M. P. Pépin and M. D. Whitmore, J. Chem. Phys. **111**, 10381 (1999).
[14] A. Chakrabarti and R. Toral, Macromolecules **23**, 2016 (1990).
[15] G. S. Grest and M. Murat, in *Monte Carlo and Molecular Dynamics Simulations in Polymer Science*, edited by K. Binder (Oxford, New York, 1995).
[16] I. Szleifer and M. A. Carignano, Adv. Chem. Phys. **94**, 165 (1996).
[17] A. Halperin, M. Tirrell, and T. P. Lodge, Adv. Polym. Sci. **100**, 31 (1992).
[18] O. V. Borisov, E. B. Zhulina, and T. M. Birshtein, Macromolecules **27**, 4795 (1994).
[19] P. Pincus, Macromolecules **24**, 2912 (1991).
[20] R. Israëls, J. M. H. M. Scheutjens, and G. J. Fleer, Macromolecules **26**, 5405 (1993).
[21] F. von Goeler and M. Muthukumar, Macromolecules **28**, 6608 (1995).
[22] O. V. Borisov, F. A. M. Leermakers, G. J. Fleer, and E. B. Zhulina, J. Chem. Phys. **114**, 7700 (2001).
[23] S.-J. Park, T. A. Taton, and C. A. Mirkin, Science **295**, 1503 (2002).
[24] F. S. Csajka, R. R. Netz, C. Seidel, and J.-F. Joanny, Eur. Phys. J. E **4**, 505 (2001).
[25] Y. Tran and P. Auroy, Eur. Phys. J. E **5**, 65 (2001).
[26] E. P. K. Currie, A. B. Sieval, M. Avena, H. Zuilhof, E. J. R. Sudhölter, and M. A. Cohen, Langmuir **15**, 7116 (1999).
[27] M. Biesalski and J. Rühe, Macromolecules **32**, 2309 (1999).
[28] M. Biesalski, J. Rühe, and D. Johannsmann, J. Chem. Phys. **111**, 7029 (1999).
[29] Y. Tran, P. Auroy, and L.-T. Lee, Macromolecules **32**, 8952 (1999).
[30] C. Amiel, M. Sikka, J. W. Schneider, Jr., Y.-H. Tsao, M. Tirrell, and J. W. Mays, Macromolecules **28**, 3125 (1995).
[31] Y. Mir, P. Auroy, and L. Auvray, Phys. Rev. Lett. **75**, 2863 (1995).
[32] H. Ahrens, S. Förster, C. A. Helm, N. A. Kumar, A. Naji, R. R. Netz, and C. Seidel, J. Phys. Chem. B **108**, 16870 (2004).
[33] G. Romet-Lemonne, J. Daillant, P. Guenoun, J. Yang, and J. W. Mays, Phys. Rev. Lett. **93**, 148301 (2004).
[34] P. Guenoun, A. Schlachi, D. Sentenac, J. W. Mays, and J. J. Benattar, Phys. Rev. Lett. **74**, 3628 (1995).
[35] H. Ahrens, S. Förster, and C. A. Helm, Macromolecules **30**, 8447 (1997).
[36] H. Ahrens, S. Förster, and C. A. Helm, Phys. Rev. Lett. **81**, 4172 (1998).
[37] U. Raviv, S. Giasson, N. Kampf, J.-F. Gohy, R. Jérôme, and J. Klein, Nature (London) **425**, 163 (2003).
[38] M. Balastre, F. Li, P. Schorr, J. Yang, J. W. Mays, and M. V. Tirrell, Macromolecules **35**, 9480 (2002).
[39] S. Hayashi, T. Abe, N. Higashi, M. Niwa, and K. Kurihara, Langmuir **18**, 3932 (2002).
[40] T. Abraham, S. Giasson, J.-F. Gohy, and R. Jérôme, Langmuir **16**, 4286 (2000).
[41] T. W. Kelley, P. A. Schorr, K. D. Johnson, M. Tirrell, and C. D. Frisbie, Macromolecules **31**, 4297 (1998).
[42] F. S. Csajka and C. Seidel, Macromolecules **33**, 2728 (2000).
[43] F. S. Csajka and C. Seidel, Macromolecules **38**, 2022 (2005).
[44] C. Seidel, Macromolecules **36**, 2536 (2003).
[45] C. Seidel, Macromolecules **38**, 2540 (2005).
[46] H. Chen, R. Zajac, and A. Chakrabarti, J. Chem. Phys. **104**, 1579 (1996).
[47] G. Orkoulas, S. K. Kumar, and A. Z. Panagiotopoulos, Phys. Rev. Lett. **90**, 048303 (2003).
[48] D. W. Cheong and A. Z. Panagiotopoulos, Mol. Phys. **103**, 3031 (2005).
[49] F. Fang and I. Szleifer, J. Chem. Phys. **119**, 1053 (2003).
[50] M. A. Carignano and I. Szleifer, Mol. Phys. **100**, 2993 (2002).
[51] F. Fang and I. Szleifer, Proc. Natl. Acad. Sci. U.S.A. **103**, 5769 (2006).
[52] R. Nap, P. Gong, and I. Szleifer, J. Polym. Sci., Part B: Polym. Phys. **44**, 2638 (2006).
[53] P. Gonzalez-Mozuelos and M. Olvera de la Cruz, J. Chem. Phys. **103**, 3145 (1995).
[54] T. Wu, J. Genzer, P. Gong, I. Szleifer, P. Vlcek, and V. Šubr, in *Polymer Brushes*, edited by R. Advincula (Wiley-VCH, New York, 2004).
[55] P. Gong, T. Wu, J. Genzer, and I. Szleifer (submitted).
[56] O. J. Hehmeyer and M. J. Stevens, J. Chem. Phys. **122**, 134909 (2005).
[57] H. F. Schmidt, IBM J. Res. Dev. **43**, 351 (1999).

Downloaded 28 Jun 2007 to 128.220.135.141. Redistribution subject to AIP license or copyright, see http://jcp.aip.org/jcp/copyright.jsp

[58] M. N. Rosenbluth and A. W. Rosenbluth, J. Chem. Phys. **23**, 356 (1955).
[59] G. Orkoulas and A. Z. Panagiotopoulos, J. Chem. Phys. **101**, 1452 (1994).
[60] A.-P. Hynninen, M. Dijkstra, and A. Z. Panagiotopoulos, J. Chem. Phys. **123**, 084903 (2005).
[61] See EPAPS Document No. E-JCPSA6-127-005725 for the detailed statistical mechanics of the Monte Carlo charged chain regrowth move in a finite geometry, implementation details, comments on counterion condensation, and tabulated results. This document can be reached via a direct link in the online article's HTML reference section or via the EPAPS homepage (http://www.aip.org/pubservs/epaps.html).
[62] D. M. Heyes, M. Barber, and J. H. R. Clarke, J. Chem. Soc., Faraday Trans. 2 **73**, 1485 (1977).
[63] A. Arnold and C. Holm, Chem. Phys. Lett. **354**, 324 (2002).
[64] E. Spohr, J. Chem. Phys. **107**, 6342 (1997).
[65] R. Shvartzman-Cohen, E. Nativ-Roth, E. Baskaran, Y. Levi-Kalisman, I. Szleifer, and R. Yerushalmi-Rozen, J. Am. Chem. Soc. **126**, 14850 (2004).
[66] P. Gong and I. Szleifer, J. Colloid Interface Sci. **278**, 81 (2004).
[67] F. J. Solis and M. Olvera de la Cruz, J. Chem. Phys. **112**, 2030 (2000).

Downloaded 28 Jun 2007 to 128.220.135.141. Redistribution subject to AIP license or copyright, see http://jcp.aip.org/jcp/copyright.jsp